# Ensemble of land-surface air temperatures between 1880-2022 using a revised pair-wise homogenization algorithm

DuoChan,[a] GeoffreyGebbie,[a] PeterHuybers,[b]

[a] *Department of Physical Oceanography, Woods Hole Oceanographic Institution, Woods Hole, Massachusetts*

[b] *Department of Earth and Planetary Sciences, Harvard University, Cambridge, Massachusetts*

*Corresponding author*: Duo Chan, duo.chan@whoi.edu

*This manuscript is a non-peer reviewed preprint submitted to EarthArXiv. It is also submitted to submitted to Journal of Climate for peer review.*

ABSTRACT: Various observational estimates of historical land surface air temperature (LSAT) trends differ on account of differences in corrections. Relative to the most-recent estimate provided by NOAA's Global Historical Climatology Network Monthly Version 4 (GHCNm4), an estimate by Berkeley Earth is 0.02°C warmer and one by the Climate Research Unit (CRUTEM5) is 0.14°C warmer between 1880–1940. Such systematic offsets can arise in LSAT records as a result of poorly-documented changes in measurement characteristics, including changes in instrumentation and movement of stations, as well as how these breakpoints are corrected for across different estimates. Building on an existing pair-wise homogenization algorithm ($PHA_0$ applied in GHCNmV4), we propose a revised version ($PHA_1$) that accounts for autocorrelation in climate variables and iteratively operates to adjust breakpoints. Tests on synthetic data generated by adding breakpoints to CMIP6 simulations and realizations from a Gaussian process indicate that $PHA_1$ outperforms $PHA_0$ in identifying small breaks and recovering accurate climate trends. Applied to unhomogenized station temperatures compiled within GHCNmV4, $PHA_1$ is shown to detect breakpoints that correspond with available station metadata. Uncertainties associated with $PHA_1$ are estimated by randomly perturbing algorithmic parameters. The continental mean temperature warming found using $PHA_1$ is consistent with that of Berkeley Earth to within estimated uncertainties, despite using a different homogenization approach. Relative to unhomogenized data, the $PHA_1$ homogenization increases 1880–2022 temperature trend by 0.18°C per century, with a 95% confidence interval of 0.11–0.24°C per century, leading to a continental mean temperature warming of 1.74°C between 1880–1889 and 2012–2021 with a 95% confidence interval of 1.63–1.90°C.

SIGNIFICANCE STATEMENT: Accurately correcting for systematic errors in observational records of land surface air temperature (LSAT) changes is critical for quantifying historical warming. Existing LSAT estimates are subject to systematic offsets associated with processes including changes in instrumentation and station movement. This study improves a pair-wise homogenization algorithm by accounting for the fact that climate signals are correlated over time. The revised algorithm outperforms the original in identifying discontinuities and recovering accurate warming trends. Applied to monthly station temperatures, the revised algorithm adjusts trends in continental mean LSAT since the 1880s to be 0.18°C per century greater relative to raw data. Our estimates are consistent with estimates from Berkeley Earth but indicate approximately 0.1°C greater warming since 1880 than those from the UK Met Office.

## 1. Introduction

Land surface air temperature (LSAT), as measured by weather stations, are crucial for monitoring long-term climate variations, but are also subject to systematic errors including those associated with changes in instrumentation, movement of stations, and changes in measurement environment (Trewin 2010). The process of detecting discontinuities in records and removing biases to recover underlying true climatic variations is generally called homogenization (Peterson et al. 1998; Costa and Soares 2009; Venema et al. 2012). Various homogenization approaches tend to find that temperature observations prior to the 1940s need to be adjusted several tenths of a degree Celsius cooler, thereby increasing the implied warming over the last century (Menne et al. 2018; Rohde et al. 2013b). Despite this agreement in the sign of adjustment, the magnitude of adjustments remain uncertain, leading to continental mean temperatures that differ by up to 0.2°C between 1880 to 1940 among existing estimates (Fig. 1).

The most commonly applied means of homogenizing LSATs is called pairwise station homogenization (Menne and Williams Jr 2009, hereafter MW09). This method, which we refer to as the original version of the pairwise homogenization algorithm, or $\mathrm{PHA}_0$, is based on comparing individual stations with its neighbors. $\mathrm{PHA}_0$ has been carefully tested and routinely used for over a decade (Menne and Williams Jr 2009; Lawrimore et al. 2011; Menne et al. 2018).

We briefly review $\mathrm{PHA}_0$, including to establish nomenclature. $\mathrm{PHA}_0$ first identifies neighbors for each station according to distance between stations or correlation coefficient in temperature series.

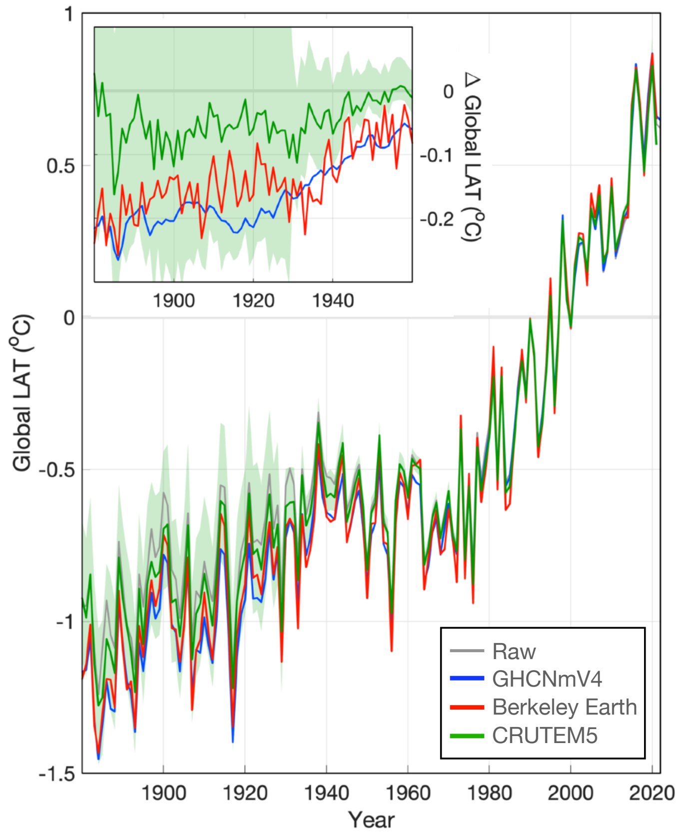


FIG. 1. **Continental mean temperature anomalies in existing estimates**. Post-1880 temperatures from raw GHCNmV4 (gray), homogenized GHCNmV4 (blue), Berkeley Earth Temperature (red), and CRUTEM5 (green). The green shading shows the 95% c.i. of a 200-member ensemble associated with CRUTEM5, derived by subtracting HadSST4 (Kennedy et al. 2019) from non-infilled HadCRUT5 (Morice et al. 2021). The upper left panel shows the adjustments to individual datasets relative to the raw GHCNmV4 estimate.

For each difference temperature series between a station and its neighbors, a standard normal homogenization test (SNHT; Alexandersson 1986) is performed to find potential breakpoints. The SNHT involves calculating the sum of the squared means of two consecutive segments of a time series,

$$T_0 = \max_{1 \leq v < n} [v \bar{z}_1^2 + (n-v)\bar{z}_2^2], \tag{1}$$

where $n$ is the length of the record, $v$ is a time index, and $\bar{z}_1$ and $\bar{z}_2$ are, respectively, the mean over months 1 to $v$ and months $v+1$ to $n$. In contrast to a weighted linear sum of the means that would be invariant to the selection of breakpoint, $T_0$ is maximized when either $\bar{z}_1$ or $\bar{z}_2$ become large. A null critical value for $T_0$ is determined by repeatedly realizing $T_0$ from randomly generated time series. As described further below, it is relevant that these time series are realized as white noise, or devoid of auto correlation. If the sample value of $T_0$ exceeds the null critical value, the time series is broken into two segment at the index $v$ that maximizes $T_0$. The test is performed iteratively between a splitting phase, where the algorithm tests whether each segment of time series contains any further breakpoints, and a merging phase, where the algorithm combines consecutive segments if the combined time series fail to pass SNHT. After this initial identification, $PHA_0$ double-checks each potential breakpoint using Bayesian Information Criteria (Schwarz 1978) to exclude cases of long-term trends and attributes confirmed breakpoints to stations that show the greatest difference with neighbors. $PHA_0$ then combines breakpoints that are temporally close to one another to account for uncertainties in the timing of identified breakpoints. Finally, an adjustment for each breakpoint is estimated by comparing the station to which a breakpoint is attributed with at least two homogeneous neighbors.

$PHA_0$ has been used to homogenize temperatures compiled under the Global Historical Climate Network Monthly Version 4 (GHCNmV4, Menne et al. 2018). In addition to central estimates generated using a default combination of $PHA_0$ parameters, an ensemble generated by perturbing algorithmic parameters in $PHA_0$ (Williams et al. 2012, hereafter WMW12) is used to quantify uncertainties in GHCNmV4 at global and regional scales. Because this GHCNmV4 homogenization ensemble is not yet publicly available, we reproduce $PHA_0$ using software made accessible from `https://www.ncei.noaa.gov/pub/data/ghcn/v3/software/`.

## 2. Apply $PHA_0$ to perturbed CMIP6 simulations

We evaluate $PHA_0$ using synthetic cases, where we introduced a fixed set of random breakpoints into temperatures from one simulation from each of 17 models from the Coupled Model Intercomparison Phase 6 (CMIP6; Eyring et al. 2016) models[1]. We use surface air temperature from the r1i1p1f1 member of each model and concatenate the historical all-forcing experiment from 1970–2015 and the SSP585 experiment from 2016–2020. Temperatures are interpolated to the location of US weather stations using a bi-linear method to retain the covariance and auto-correlation

[1]Models we use are: ACCESS-CM2, CAMS-CSM1-0, CMCC-CM2-SR5, E3SM-1-1, EC-Earth3, EC-Earth3-Veg, EC-Earth3-Veg-LR, FGOALS-f3-L, FGOALS-g3, FIO-ESM-2-0, INM-CM4-8, INM-CM5-0, MIROC6, MRI-ESM2-0, NESM3, NorESM2-LM, and NorESM2-MM.

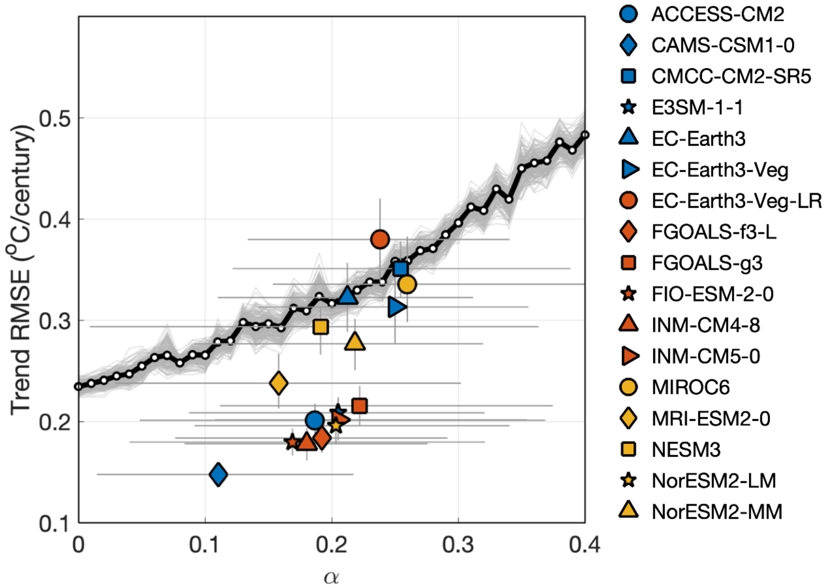


FIG. 2. **The skill of the original pair-wise station homogenization algorithm (PHA$_0$) decreases with auto-correlation of climatic signals**. The skill of PHA$_0$ is quantified using the station-wise root mean squared error (RMSE) of long-term trends over the continental US after adjustment for 17 CMIP6 models (markers) and synthetic analyses (black circles connected by a line). RMSE increases with the lag-1 auto-correlation ($\alpha$) in the difference temperature series between neighbors. The horizontal bar on each marker represents the 95% confidence interval for values of $\alpha$ across individual stations, and the vertical bar is the 95% confidence interval for mean RMSE over all stations. The confidence interval of RMSE is estimated by bootstrapping blocks of 100 stations with replacement.

structures in temperature field. A set of randomly timed breakpoints having random magnitudes are then introduced to each simulation. Appendix A contains details regarding the distribution of breakpoint timing and magnitude.

Breakpoints are identical across models but the skill of PHA$_0$ in recovering temperature trends, as measured by station-wise root mean square error (RMSE), varies widely across models (Fig. 2). CAMS-CSM1-0 has the lowest RMSE at 0.15 °C per century (1 s.d.), whereas EC-Earth3-Veg-LR has the highest RMSE at 0.38 °C per century. We present evidence that the differences in the skill of PHA$_0$ across models relates to differences in the auto-correlation of temperatures. Higher auto-correlation leads to a higher chance of realizing values of $T_0$ that exceed the critical value by chance. There is a strong correlation across model of 0.76 between the mean lag-1 auto-correlation in the difference temperature series between neighboring stations, referred to as $\alpha$, and the RMSE between inferred and actual temperature trends (Fig. 2).

To further investigate the relationship between $\alpha$ and the performance of $PHA_0$, we conduct synthetic analyses using spatially and temporally correlated temperatures. Synthetic temperatures are generated from a multivariate Gaussian process with fixed $\alpha$ values across all stations (see Appendix A for details). Synthetic ensembles having larger $\alpha$ are systematically associated with higher RMSE, a trend also shown across CMIP6 simulations (Fig. 2), suggesting that differences in auto-correlation are a primary explanation for cross-model differences in skill. These results suggest that accounting for auto-correlation in climate signals may improve the skill of $PHA_0$ in detecting breakpoints and recovering long-term temperature trends. In this study, we test whether a revised algorithm that accounts for auto-correlation shows improved skill.

We also explore another modification to $PHA_0$ that may improve its performance. $PHA_0$ is only run once and could miss breakpoints, especially if multiple stations in a region, with some containing simultaneous but small breakpoints. Changes in measurement time and instrumentation that may be associated with breakpoints are known to be pervasive at least in the US weather network (Menne and Williams Jr 2009; Williams et al. 2012). The possibility of clustered breaks suggests using an iterative approach for breakpoint identification.

## 3. A revised pair-wise station homogenization algorithm

Our revised pairwise station homogenization algorithm, $PHA_1$, is described briefly here in terms of revisions relative to $PHA_0$ (Fig. 3a) and in more detail in Appendix B. The most significant revision in $PHA_1$ involves accounting for auto-correlation in temperature differences between stations during the identification of potential breaks. The thresholds of $T_0$ in SNHT is made a function of both series length, $n$, and lag-1 auto-correlation, $\alpha$.

To estimate critical values, we model temperature difference time series as an auto-regressive order one process,

$$X_{t+1} = \alpha X_t + \epsilon. \tag{2}$$

In Eq. 2, $\alpha$ is the system memory and $\epsilon$ is white noise drawn from a standard normal distribution, $N(0,1)$. We explore values of $\alpha$ between 0 to 0.4, a typical range across CMIP6 simulations, and

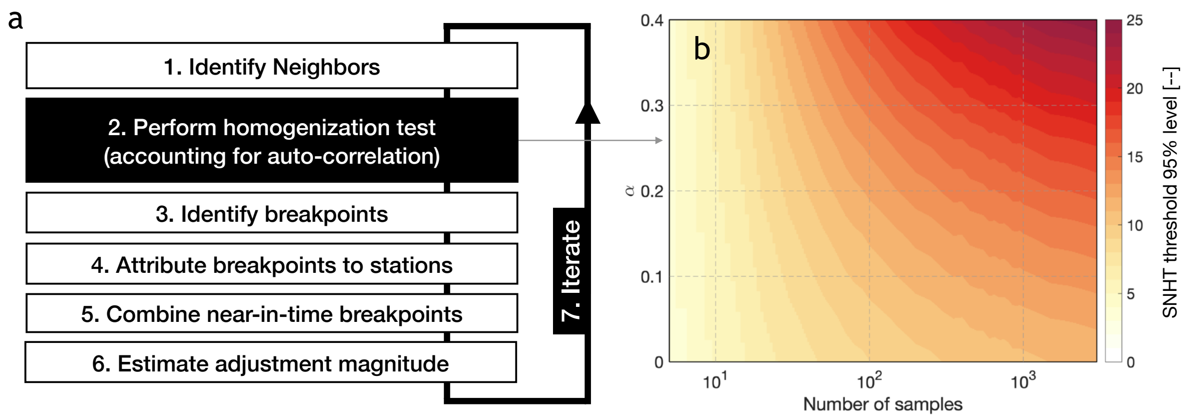


FIG. 3. **Schematic of PHA$_1$ – our revised pairwise homogenization algorithm**. (a) stream flow of individual steps in the revised algorithm. Steps different from PHA$_0$ are in black boxes. (b) Critical value of standard normal homogeneous tests. 95% critical value (heat map) shown as a function of time series length ($n$, x-axis) and lag-1 auto-correlation (y-axis).

values of $n$ between 5 and 3500. For each combination of $\alpha$ and $n$, we generate 50,000 random series and normalize each to calculate the SNHT statistics $T_0$ following Eq. 1. Higher values of $\alpha$ give greater autocorrelation and increased SNHT statistics. For example, the 95th percentile of $T_0$ for $\alpha$ equals to 0.3 and is up to 1.8 times of that when $\alpha$ equals zero (Fig. 3b).

To estimate $\alpha$ for difference series that contain potential breakpoints, we use a sliding window because breakpoints in a time series tend to bias estimates high and because shorter segments generally have fewer breaks. Assuming $\alpha$ is temporally stationary but that a time series may contain outliers associated with breakpoints, we use the median of calculated $\alpha$ values from the sliding window analysis. The length of the window is the shorter interval between 100 months and one third of the time series. To account for a potential overestimation due to multiple breakpoints, we update $\alpha$ in each splitting phase of SNHT by excluding windows overlapping with any detected breakpoints.

Following the discussion near the end of section 2, after estimating and performing adjustments (step 7), we also run a second iteration of the algorithm (step 8) to check for breakpoints relative to neighbors whose breakpoints may have been adjusted in the first iteration.

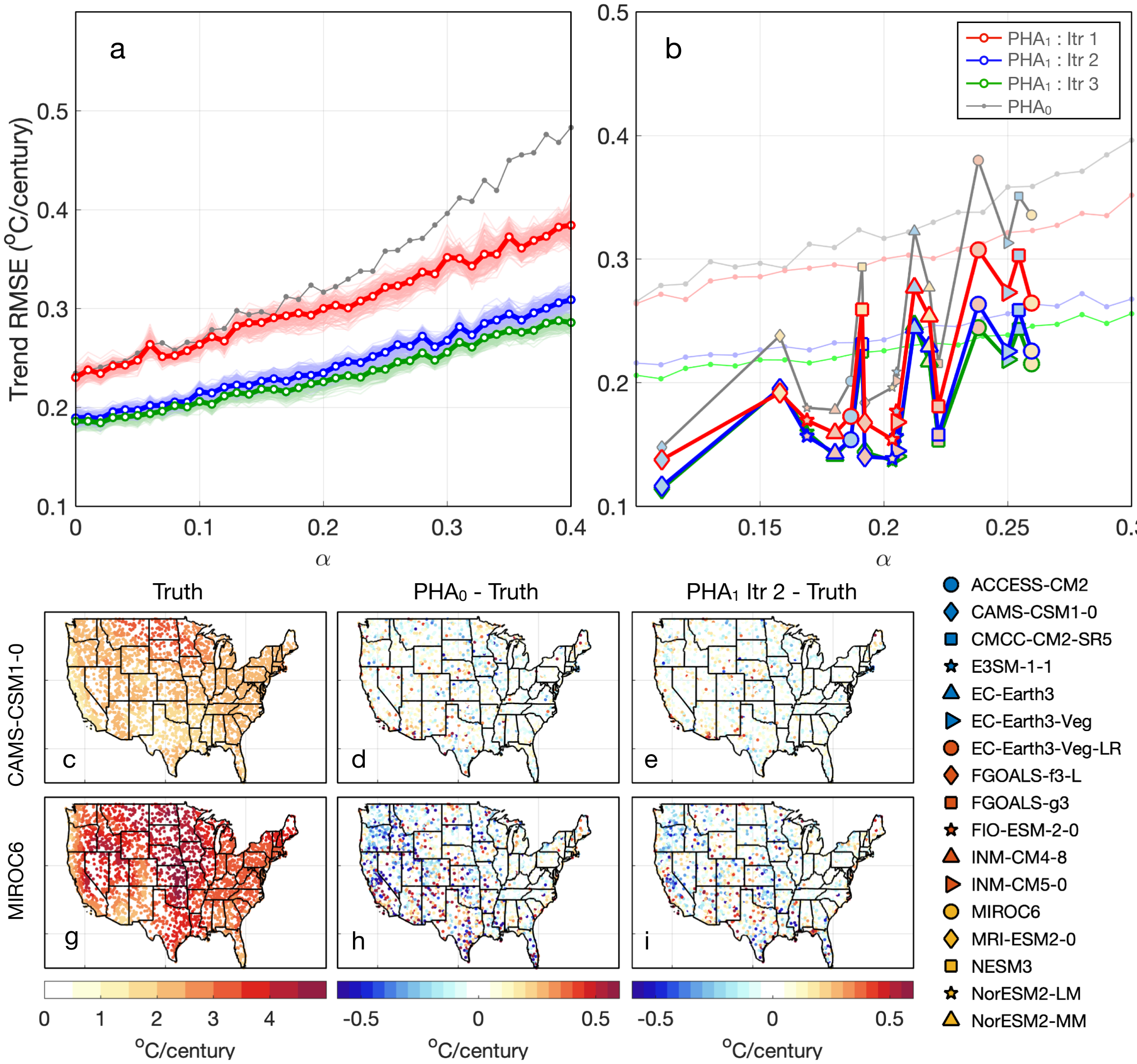


FIG. 4. **Skill of the revised pair-wise station homogenization algorithm ($PHA_1$) in recovering long-term temperature trends**. (a) RMSE in temperature trends for the Multivariate Gaussian Process ensemble after running $PHA_1$ for one (red), two (blue), and three (green) iterations. Results from $PHA_0$ (gray) are included for comparison. (b) Similar to (a), but for the CMIP6 ensemble, with the number of iterations denoted using colors of the edge of markers. Results from $PHA_0$ (gray) and the Multivariate Gaussian Process ensemble (thin lines) are also shown for comparison. Note that panel (a) and (b) have different axis ranges. (c-i) Maps of long-term trends. Each column shows trends for simulated temperatures, errors of $PHA_0$, and errors of $PHA_1$ with two iterations. The upper row displays results from CAMS-CSM1-0, the model with the lowest auto-correlation, while the lower row shows results from MIROC6, the model with the highest auto-correlation.

## 4. Applying $PHA_1$ to simulations and synthetic data

We first assess the skill of $PHA_1$ relative to $PHA_0$ using perturbed CMIP6 simulations and a synthetic data ensemble generated from a multivariate Gaussian processes (MGP). We show that each revision in $PHA_1$ improves skill. We also show that the reason for improved skill is that $PHA_1$ correctly identifies more breakpoints while being subject to fewer false alarms, or false alarms that are of small magnitude and, thus, have little effect on long-term trends. Unless otherwise stated, $PHA_1$ is run using a default parameter combination as in Williams et al. (2012, also listed as ensemble 1 in Table B2).

### *a. RMSE of Long-term Trends*

To evaluate the performance of $PHA_1$, we begin by comparing the root mean square error (RMSE) of long-term temperature trends between $PHA_1$ and $PHA_0$ on the MGP-based synthetic ensemble (Fig. 4a). After a single iteration, trend RMSE values in $PHA_1$ are, on average, 0.30 °C per century, a value that is 0.03°C per century lower than $PHA_0$. The reduction in RMSE increases with the strength of the auto-correlation, $\alpha$, from zero when $\alpha$ is zero to 0.10°C per century when $\alpha$ is 0.4. Running $PHA_1$ multiple times leads another systematic reduction in RMSE that is less dependent on auto-correlations. The second iteration of $PHA_1$reduces RMSE, on average over $\alpha$ from zero to 0.4, by 0.06°C per century. A third iteration only leads to diminishing further reduction by, on average, 0.01°C per century.

The improvement in skill shown by $PHA_1$ is consistent when applied to perturbed CMIP6 simulations (Fig. 4b). When running $PHA_1$ for one iteration, the reduction in RMSE ranges from 0.01°C per century in CAMS-CSM1-0 (the model with the lowest $\alpha$) to 0.07°C per century in EC-Earth3-Veg-LR (the model with the forth highest $\alpha$). The fact that the RMSE reduction across CMIP6 models nearly follows a one-to-one relationship with that of the MGP synthetic ensemble indicates that $PHA_1$ improves trend recovery regardless of the underlying temperature evolution and regardless of the distribution of $\alpha$ across regions within a simulation. Running $PHA_1$ multiple times further reduces RMSE in the CMIP6 ensemble, with an average reduction of 0.03°C per century for the second iteration and no significant changes for the third. Together with reduced RMSE, $PHA_1$ also increases the spatial correlation of long-term trends from an average of 0.95 across models in $PHA_0$ to 0.97 in $PHA_1$ with two iterations (Fig.4 c-l).

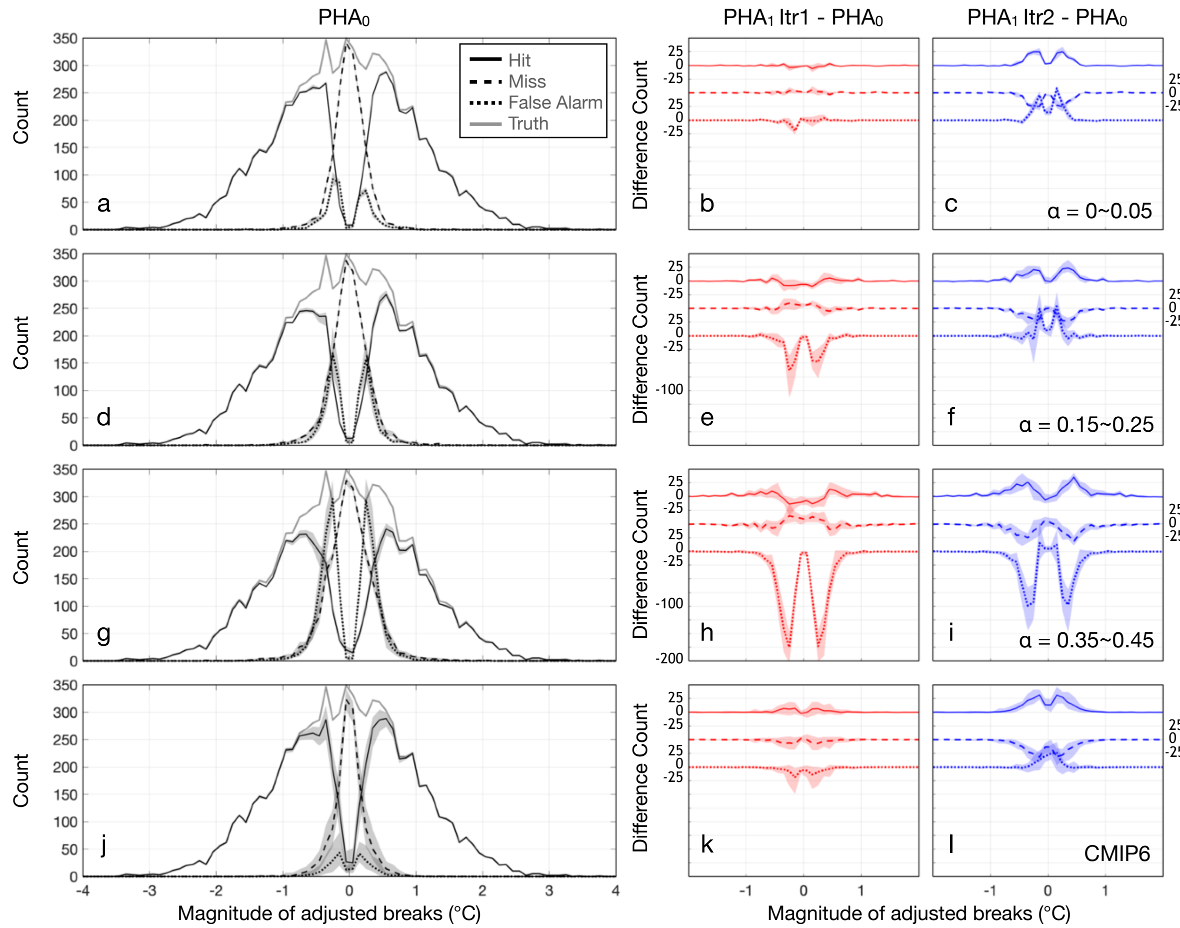


FIG. 5. **The identification of breakpoints using the histograms of hits, misses, and false alarms**. The left column shows the histogram of hits (solid), misses (dashed), and false alarms (dotted) using $\text{PHA}_0$. The middle column shows the difference between $\text{PHA}_1$ with one iteration minus $\text{PHA}_0$. Lines are offset for visibility. The right column is as the middle but for $\text{PHA}_1$ with two iterations. From top to bottom, each row shows synthetic analyses for $\alpha$ = 0–0.05, $\alpha$ = 0.15–0.25, $\alpha$ = 0.35–0.45, and the CMIP6 ensemble. The shadings indicate the range across MGP ensemble members or CMIP6 models.

### *b. Hits, Misses, and False Alarms*

Improved skill in $\text{PHA}_1$ comes from decreasing the number of false alarms and better identifying breakpoints. To demonstrate improvements in breakpoint identification, we develop a scoring system by counting the number of hits, misses, and false alarms. Specifically, a hit is if a breakpoint is identified within a one-year epoch that centers on the timing of a true breakpoint. If two epochs overlap, the overlapping months are assigned to the epoch of the nearest true break. Breakpoints identified outside of an epoch are considered false alarms, and epochs not identified to have a breakpoint are misses. When an epoch contains multiple identified breakpoints, the breakpoint with the highest estimated magnitude is taken as a hit and others as false alarms. The length of this epoch does not qualitatively change our results.

The improvement associated with running $PHA_1$ for the first iteration comes mainly from reducing false alarms. As $\alpha$ increases, $PHA_0$ makes fewer hits but significantly more false alarms. Among the 8188 introduced breaks, the number of hits decreases from 6476 when $\alpha$ = 0 to 5727 when $\alpha$=0.4, whereas false alarms increases from 426 to 1785 (Fig. 5a,d,g). When $\alpha$ = 0, $PHA_1$ behavior is the same as $PHA_0$ (Fig. 5b). However, as $\alpha$ increases, $PHA_1$ apparently makes fewer false alarms then $PHA_0$, with 260 fewer when $\alpha$ = 0.2 (Fig. 5e) and 1057 fewer when $\alpha$ = 0.4 (Fig. 5h). Such a reduction is consistent with accounting for auto-correlations, which uses a higher $T_0$ threshold and prevents SNHT from mis-identifying large climatic variations as breakpoints. On the other hand, we find no apparent change in the number of hits or misses (Fig. 5e,h).

The improvements associated with running $PHA_1$ for the second iteration comes mainly from increasing the hit rate. Over all $\alpha$ values examined, $PHA_1$ with two iterations makes 211 [168, 273] (95% c.i.) more hits than $PHA_0$ (Fig. 5c,f,i). There is, however, a trade-off between increasing the hit rate and increasing the rate of false alarms (Fig.5c, f, i). That said, the median absolute magnitude of additional hits is 0.20°C, as compared to 0.14°C for false alarms. As a result, the effect of increasing hitting rate wins, and running a second iteration still reduces RMSE. Qualitatively similar decreases in false alarms and increases in the hit rate are also found in the CMIP6 ensemble (Fig. 5j–l).

## 5. Analysis of GHCN monthly temperatures

Having established that $PHA_1$ shows improvements in skill in trials on synthetic data, in this section, we apply it to monthly air temperatures compiled within the Global Historical Climatology Network (GHCNM) version 4 (Menne et al. 2018). GHCNmV4 contains monthly mean temperatures from approximately 27,850 stations (Fig. 6c). The number of stations increases from the 1850s to the 1970s, plateaus from the 1970s to the 2000s, and declines thereafter (Fig. 6b). Records prior to the 1900s are mainly from Europe, US, India, coastal Australia, and Japan (Fig. 6d). More

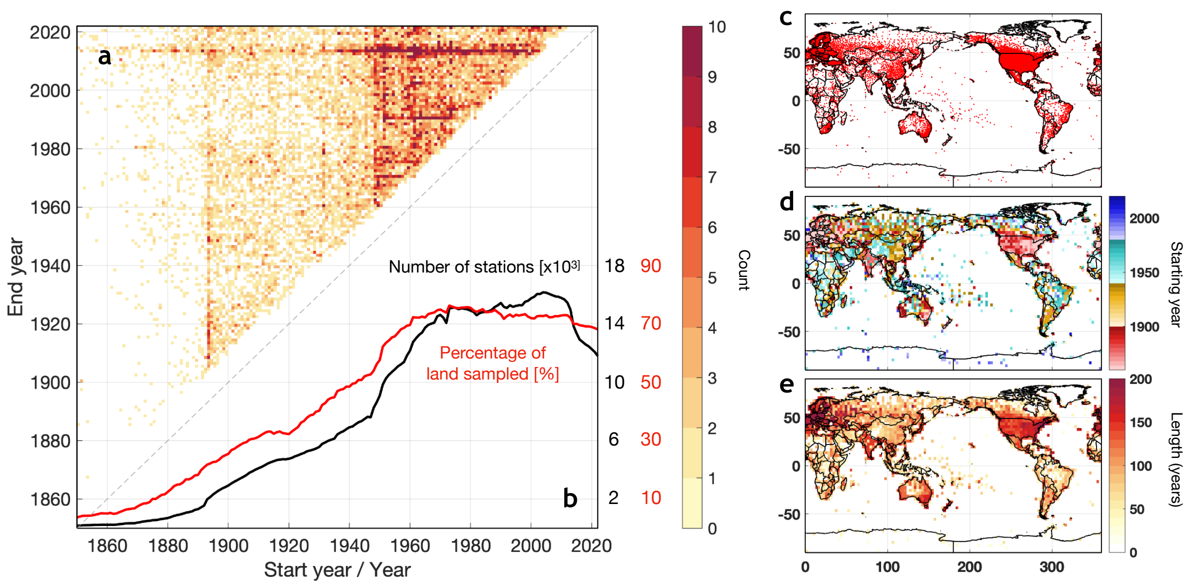


FIG. 6. **Statistics of GHCNmV4.** (a) Histogram of the starting and ending year of weather stations used in this study (heat map). (b) Number of stations as a function of year (black, unit: thousand stations) and the percentage of land areas sampled (red). This percentage is calculated after binning the station coverage to 3°×3° grids. (c) Distribution of all 27,618 weather stations used. (d) The earliest sampled year in each 3°×3° grid box. (e) The length of sampled period of each grid box.

than 3000 stations have records longer than 100 years (Fig. 6a&e). Despite the recent drop in total number of stations, the percentage of sampled land area, calculated by counting 3°×3° grid boxes, remains approximately 70% throughout the past sixty years (Fig. 6b). To perform an initial quality screening, we exclude records having QC flags that identify possible issues including duplication, outlier behavior, spatial inconsistency, and isolation (Menne et al. 2018), such that our analysis is based on 27,808 stations.

### *a. Breakpoint Detection and Temperature Adjustments under the Default Parameter Combination*

Under the default parameter combination (Table B2, ensemble 1), applying $PHA_0$ to the quality-controlled stations leads to identification of 63,492 breakpoints between 1880 to 2023. In comparison, Menne et al. (2018) reported NOAA's homogenized GHCNmV4 product contains approximately 71,000 breaks from 1880 to 2016. We are unsure as to the origin of the discrepancy in the

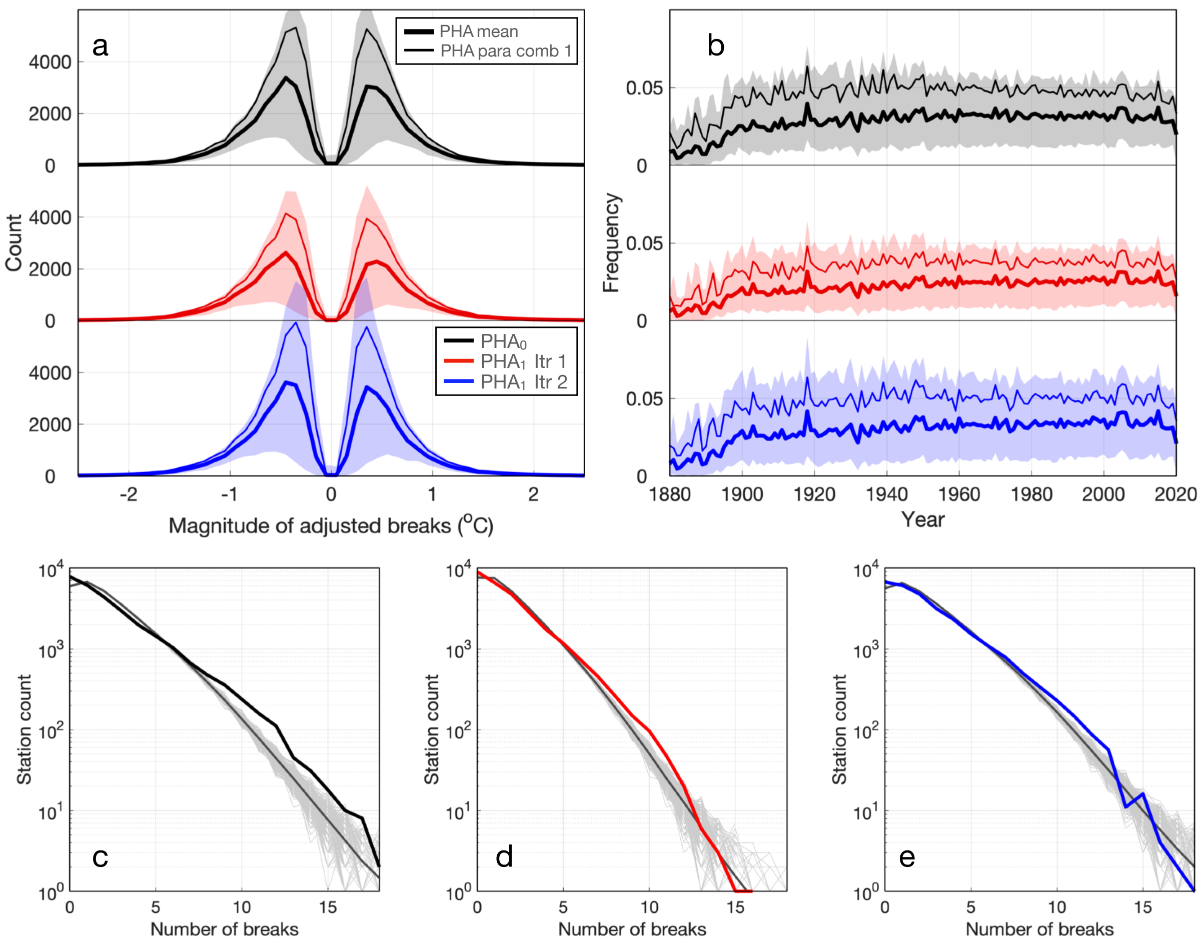


Fig. 7. **Adjusted breakpoints in GHCNmV4**. (a) Histogram of the magnitude of adjusted breakpoints for $PHA_0$ (black) and $PHA_1$ running for one (red) and two iterations (blue). Results are for the default parameter combination (solid curves) and 95% c.i. (shadings) across a 200-member ensemble. (b) as a, but for rate of adjusted breakpoints. (c-e) histogram of detected number of breaks in each station (thick curves) for $PHA_0$ (c), $PHA_1$ with one (d), and $PHA_1$ with two iterations under the default parameter combination (e). Also shown are the mean count (gray curve) over a 500-member ensemble generated from binomial distributions, assuming the occurrence of breakpoints within a station is independent in time (null-hypothesis). The light gray lines show individual members of the binomial ensemble.

number of reported breaks, though one possible reason is that we do not use metadata in our PHA analyses. Nevertheless, we have made the $PHA_0$ code we run and detailed results available in order to facilitate inter-comparison going forward. Running $PHA_1$ with the same parameter combination

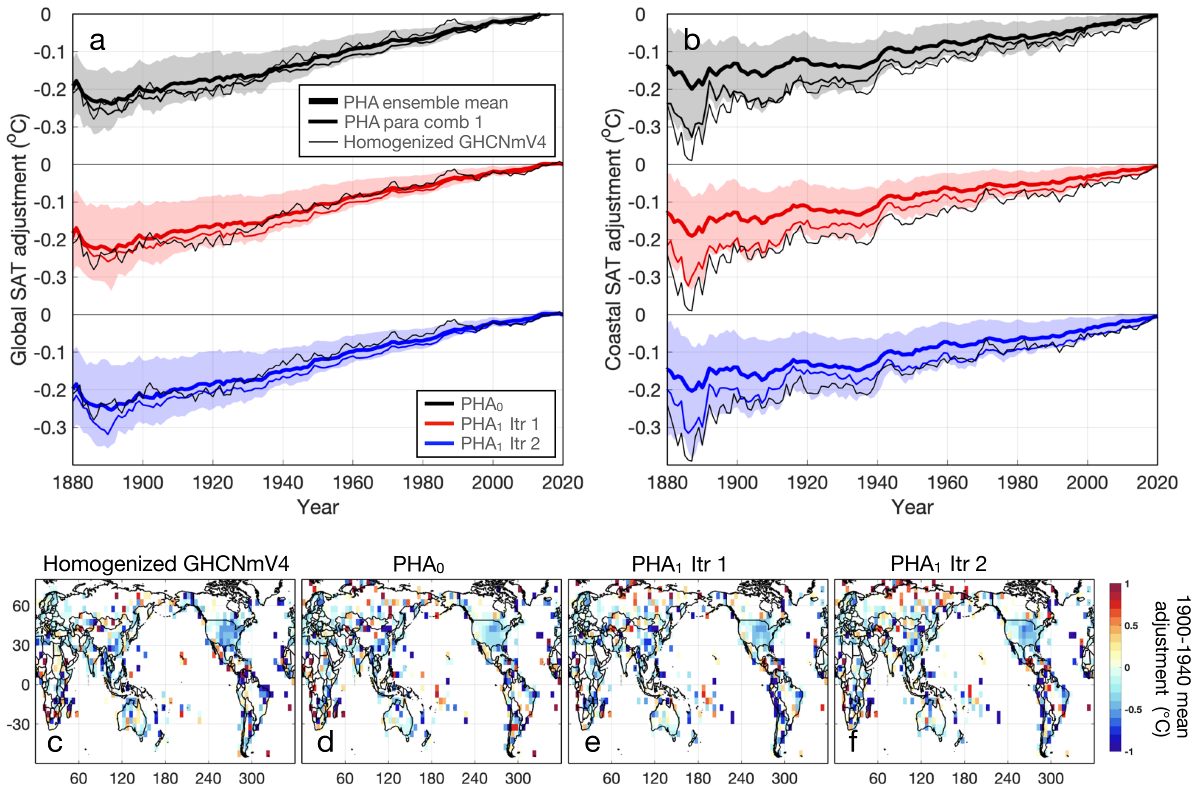


FIG. 8. **Adjustments at global and regional scales**. (a) Continental-mean station adjustments for $PHA_0$ (black) and $PHA_1$ running for one (red) and two iterations (blue). Results are for the mean over a 200-member parameter perturbation ensemble (thick colored curves) and the default parameter combination (thin colored curves). Shadings show 95% c.i. across the 100-member ensemble. Also show is the adjustment in homogenized GHCNmV4 (thin black curve). (b) as a, but for coastal mean adjustments. (c-f) spatial distribution of 1900-1940 mean adjustments for homogenized GHCNmV4 (c), $PHA_0$ (d), $PHA_1$ with one (e), and PHA with two iterations (f).

gives 50,105 breakpoints between 1880–2023 using one iteration. A second iteration of $PHA_1$ identifies an additional of 16,894 breaks whose median adjustment magnitude is 0.29°C (Fig. 7a).

Similar to Menne et al. (2018) and $PHA_0$, $PHA_1$ detects more negative than positive breakpoints, and the mean of detected breaks for two iterations is negative (Fig. 7a). It follows that continental mean temperature adjustments show positive linear trends of 0.19 and 0.21°C per century over 1880–2022 for respective iterations of $PHA_1$ (Fig. 8a). These trends are qualitatively consistent with the 0.19°C per century found using $PHA_0$ and reported for the GHCNmV4 product (Fig. 8a).

The spatial pattern of our adjustments in the early 20th century (Fig. 8e,f) is generally negative across the globe, with apparent patches of negative values over the Eastern US, Alaska, coastal South America, Eastern China, and Europe. Positive adjustments are found over Siberia, Hawaii, and part of Africa. Compared with NOAA's homogenized GHCNmV4 (Menne et al. 2018), the mean adjustment over three iterations is smaller over, for example, the central and eastern US (Fig. 8d). That said, $PHA_1$ still captures the spatial distribution of data biases estimated by Menne et al. (2018), with the spatial correlation between the two patterns of 1900–1940 mean adjustments being 0.57 (Fig. 8c-f).

### *b. Comparison with Station Metadata*

The frequency of detecting breakpoints is consistent throughout the 20th century, with the first iteration detecting breaks at an average rate of once per 25 years of station data (red curve in Fig. 7b). This rate increases to about once per 20 years after running an additional iteration.

Some level of breakpoints are expected. For example, the US historical climate network has experienced a shift from liquid in glass (LiG) thermometers in Stevenson screens to the electronic resistance thermometer known as the Maximum-Minimum Temperature Sensor (Menne and Williams Jr 2009; Williams et al. 2012).

To more-specifically examine the rate and pattern of breakpoints that are algorithmically identified, we compare detected breakpoints with potential breaks suggested by available station history data compiled under the Historical Observing Metadata Repository (HOMR, `https://www.ncei.noaa.gov/access/homr/`), and record, for each station, the timing when metadata suggests potential changes in temperature measurement technique or location. A total of four categories of metadata information are investigated: segmented location information, record relocation, segmented temperature information, and recorded instrument changes. Station metadata is limited. Among the 27,755 GHCNmV4 stations, only 10,227 have metadata indicating at least one potential discontinuity throughout their entire station history, and more than 99% of these stations are from the US or US affiliated islands.

The rate at which available metadata indicates potential discontinuities varies with time, and the temporal evolution is unique among different sources of information. For example, relocation rates increase in the late 1930s, drop in the 1970s, and again peak in the 1990s and 2000s (Fig. 9b). On

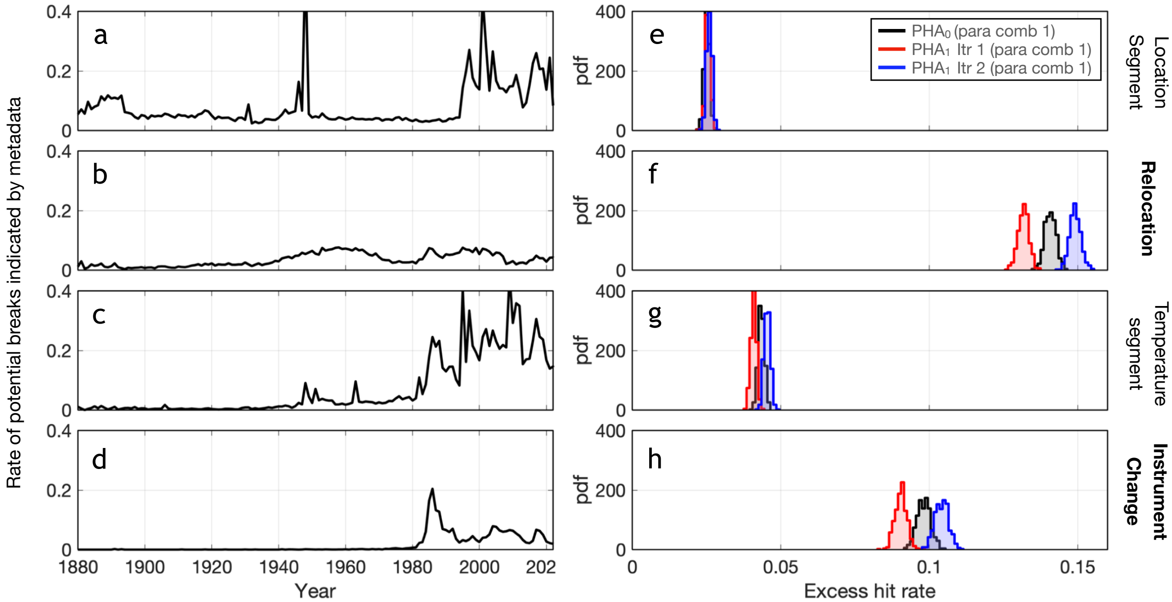


FIG. 9. **Comparison with metadata**. (a-d) frequency of metadata-suggested potential breaks when using (a) segmented location information, (b) recorded relocation, (c) segmented temperature information, and (d) recorded instrument changes. (e-h) excess hit rate of PHA$_0$ (black), PHA$_1$ with one (red), and PHA$_1$ with two iterations (blue). The excess rate is relative to a null hypothesis that adjustments are made at random timing.

the other hand, instrument changes are rare before they peak in the 1980s (Fig. 9d). We are unaware of whether changes in reported rates among the records with station data reflect changes in the actual rates of relocation and instrumentation change or, instead, the recording of such changes. For this reason, we only focus on the rate at which metadata-indicated discontinuities correspond with identified breakpoints. Specifically, if a metadata-indicated discontinuity lies within the 1-year epoch of detected breaks, as defined in section 4, we count it as a hit. For purposes of comparison, we also estimate a null-hypothesis hit rate, where meta-data adjustments occur at random timing. The null is constructed by randomly shuffling the timing of metadata-indicated discontinuities within each station and repeating the process 1000 times to obtain a distribution.

The hit rate of meta-data indicated changes with PHA identified breakpoints is significantly higher than expectations from randomized meta-data for each category of metadata ($P$ <0.001), indicating the skill of PHA-based methods. Averaging across stations and PHA approaches, the correspondence of meta-data indicated changes with breakpoints is 3%, 14%, 4%, and 10% higher than adjustments with random timing for segmented location information, record re-location, segmented temperature information, and recorded instrument changes, respectively (Fig. 9e-h). These results suggest that moving stations and changing measurement approaches are more likely to result in identifiable breakpoints. Moreover, although $PHA_1$ with one iteration generally yields lower excess hit rate than $PHA_0$, $PHA_1$ running for two iterations gives a higher hit rate than $PHA_0$ for all metadata types. These results help confirm the skill of $PHA_1$.

It can also be emphasized, given that 94% of breakpoints identified by $PHA_1$ are not associated with an event indicated by relocation or instrumental changes, that using a homogenization algorithm is important for uniform treatment of the data. This inference is already obvious, however, in that even in the U.S. where most meta-data is available, meta-data rates (relocation or instrumental change) range from 2% per year between 1900–50 and 8% per year between 1980–2023, whereas the ratio of PHA-identified breakpoints between these two intervals remains relatively stable at about 6% per year.

Although the rate of PHA-detected breakpoints is stable in time, stations with one breakpoint are more likely to experience other breaks. To demonstrate this point, we compare the number of breaks per station between GHCN and a null hypothesis assuming the occurrence of breakpoints is independent across time and stations. To construct this null hypothesis, we draw, for each station, a number of breakpoints from a binomial distribution $B(p_B, n_B)$, where the success rate or average percentage of years having breaks is $p_B$ and $n_B$ is the number of years with data. We repeat the process 500 times to obtain a distribution assuming independent breakpoint occurrence. GHCN homogenized using either $PHA_0$ or $PHA_1$ has significantly more stations without breaks, fewer stations with fewer than six breakpoints, and more stations with seven or more breakpoints (Fig. 7c–f). A possible explanation involves that some discontinuities detected by $PHA_0$ are associated with problematic segments that recover later in time, such that breakpoints may have the tendency of appearing in pairs.

### c. *Uncertainty Quantification*

Similar to Williams et al. (2012), we use an ensemble method to quantify parametric uncertainties in $PHA_1$ associated with errors in the timing of breakpoints and the magnitude of required adjustments. That is, in addition to the default parameter combination, we randomly perturb all parameters in the algorithm (Table B1). Note that randomized parameter combinations tend to give higher error rates, often because of conservative breakpoint adjustments that relax the magnitude of trend adjustments towards zero (Williams et al. 2012). To account for this potential bias, we first run a 500-member randomized parameter ensemble on the MGP synthetic data where $\alpha = 0.2$, the median across CMIP6 models. The resulting mean station-wise RMSE over two iterations ranges from 0.24 to 2.12°C per century, while the default combination gives an RMSE of 0.27°C per century. The high error for some combinations is associated with insufficiently adjusting breaks, which could be associated with SNHT identifying too many or too few breakpoints in the initial screening. Whereas too few initial breakpoints naturally results in fewer adjustments, too many initial breakpoints would result in insufficient numbers of homogeneous neighbors required for estimating adjustments. We then subset the 100 combinations that gives the lowest RMSE (Table B2) and run with each combination with up to two iterations to generate a 200-member LSAT ensemble. The RMSE of the 100 used combinations ranges from 0.24 to 0.39 °C per century, with 11 giving lower RMSE than the default combination.

Applying the trimmed parameter ensemble to GHCNmV4, we detect 32,216 [11,458, 61,581] (median and range across 100 parameter combinations) and 43,386 [14,605, 83,769] breakpoints for one and two iterations, respectively (Fig. 7a). The mean of detected breakpoints ranges between -0.12 and -0.04°C. Thus, accounting for timing and magnitude uncertainties still suggests that the raw GHCNmV4 underestimates long-term trends in temperature warming on continental and global scales. Estimated global-average adjustments have 1880–2022 trends ranging between 0.08 and 0.27 °C per century (Fig. 8a). Note that, compared with estimates using the default parameter combination, 0.19 and 0.21°C per century for one and two iterations respectively, the uncertainty estimate is asymmetric, but less than would be the case if not first sub-selecting for plausible parameter combinations. It is also worth noticing that although the homogenized GHCNmV4 is consistent with our ensemble for continental mean temperatures (Fig. 8a), the adjustments found in homogenized GHCNmV4 for coastal stations are more negative than our ensemble throughout 1880–2023 (Fig. 8b). In a recent paper, we showed that discrepancies exist between SSTs and LSATs near coastlines during the early 1900s (Chan et al. 2023). An associated implication is that, if coastal LSATs are used to estimate biases in sea-surface temperature (SST) measurements, using

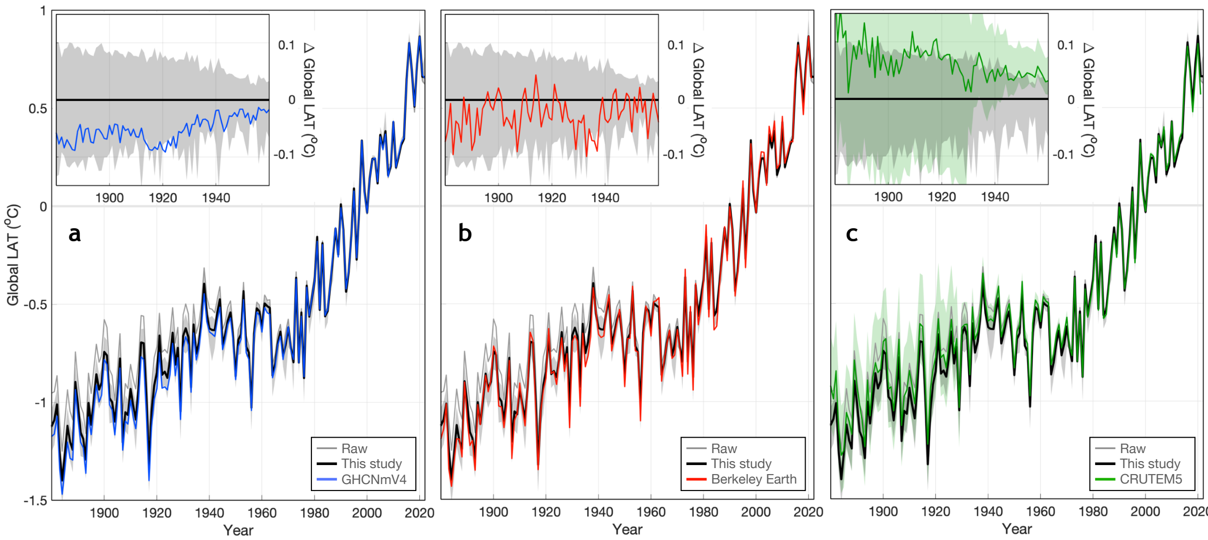


FIG. 10. **Comparison of continental mean temperature anomalies with existing estimates**. (a) Homogenized temperatures using our revised algorithm (black), homogenized GHCNmV4 (blue), and raw GHCNmV4 (gray). Anomalies are relative to the mean over 1982–2014 and are calculated using a pairing and matching algorithm following Chan et al. (2023). Shading shows the 95% confidence interval over the 200-member ensemble. Coverage uncertainties are not accounted. Shown in the panel on the left top corner is the difference from the central estimate of our adjusted temperatures. (b) as a, but for comparison with Berkeley Earth Temperature (red). Berkeley temperature is masked to have the same data coverage as GHCNmV4. (c) as a, but for CRUTEM5 (green). The green shading shows the 95% c.i. over a 200-member ensemble derived from subtracting HadSST4 (Kennedy et al. 2019) from non-infilled HadCRUT5 (Morice et al. 2021).

homogenized GHCNmV4 would result in an SST trend that is about 0.07°C per century higher than using our LSAT ensemble.

## 6. Discussion and Conclusion

To further improve the detection and adjustment of discontinuities in historical temperature records from weather stations, we propose a revised pairwise homogenization algorithm that accounts for auto-correlation in time series. Testing on perturbed CMIP6 simulations and synthetic data with different levels of autocorrelation indicates that our revised algorithm identifies more breaks and generally produces fewer false alarms, thereby showing better skill in recovering long-term temperature trends. We are also able to show a significant relationship between events recorded in metadata and breakpoints found using $PHA_1$.

Applying $PHA_1$ to unhomogenized GHCNmV4 station temperatures increases the 1800–2022 trend in continental mean temperature by 0.18 [0.11, 0.27]°C per century (95% c.i.). Our estimates suggest that the continental mean temperature over 2012–2021 has been 1.74 [1.63, 1.90]°C (95% c.i.) warmer than the 1880s. The uncertainty of our estimates is quantified using a 200-member ensemble that accounts for parametric uncertainties of $PHA_1$. The code and detailed results of our algorithm are publicly accessible at `https://doi.org/10.7910/DVN/AA0OM0`.

We compare our continental mean temperatures with three existing estimates (Fig. 10) from GHCNmV4 (Menne et al. 2018), Berkeley Earth (Rohde et al. 2013a), and CRUTEM5 (Osborn et al. 2021). To facilitate direct comparison, we average only over grid boxes where all products have observations after re-gridding to the CRUTEM5 5x5° resolution. GHCNmV4 is closely consistent with our $PHA_1$-based ensemble after the 1960s. Between 1880 to 1940, however, GHCNmV4 is at the 10th percentile of our estimates (Fig. 10a), implying greater warming between the 1880s and 2012–2021 at 1.82°C than the central estimate from $PHA_1$.

In contrast, CRUTEM5 has a central estimate that is at the 95% quantile of the $PHA_1$-based ensemble between 1880 to 1940 (Fig. 10c). This discrepancy leads CRUTEM5 to show the least amount of warming since the 1880s of only 1.62 [1.38, 1.81]°C. Such differences may arise from the fact that CRUTEM5 used homogenization efforts by national or regional initiatives as opposed to a global statistical algorithm (Osborn et al. 2021). Note that CRUTEM5 also makes an ensemble characterization of uncertainties publicly available. In addition to the homogenization uncertainties that we account for, the CRUTEM5 ensemble also accounts for sampling and measurement errors within individual grid boxes and instrumental exposure biases from nonstandard screenings (Osborn et al. 2021), leading to a larger 95% confidence interval, particularly prior to the 1930s.

The Berkeley Earth temperature estimate is closely consistent with our ensemble throughout 1880–2022 (Fig. 10b) and indicates a warming of 1.78 °C since the 1880s. Note that Berkeley Earth temperature detects breakpoints using a method similar to step 1–5 of $PHA_0$, but rather than explicitly adjusting temperatures, it simply splits records into two descendants containing data before and after detected breakpoints and treat them as different records when calculating temperature anomalies relative to some climatological periods (Rohde et al. 2013a). On account of the greater skill shown by $PHA_1$ than $PHA_0$ and consistency with the Berkeley Earth temperature dataset, we suggest that the present ensemble gives a credible — and, arguably, the most credible — estimate of LSAT warming since 1880. It will be useful to integrate these land-based estimates of warming with recent and ongoing work to combine land and sea-surface temperature datasets (e.g. Cowtan et al. 2018; Chan et al. 2023) as well as to infill for missing regions (Kadow et al. 2020; Meinshausen et al. 2022, e.g.) in order to obtain consistent estimates of global temperature.

*Acknowledgments.* D. Chan is supported by the Woods Hole Oceanographic Institute Weston Howland Jr. Postdoctoral Fellowship. G. Gebbie is supported by NSF OCE-82280500. P. Huybers is supported by NSF Grant 2123295. The authors have no conflict of interests to declare.

*Data availability statement.* All datasets used in this study are available as follows: GHCNmV4 (`https://www.ncei.noaa.gov/pub/data/ghcn/v4/`; last access, May. 31, 2023). HOMR (`https://www.ncei.noaa.gov/access/homr/`; last access, May. 31, 2023). Berkeley Earth Monthly temperature (`https://berkeley-earth-temperature.s3.us-west-1.amazonaws.com/Global/Gridded/Complete_TAVG_LatLong1.nc`; last access, Jul. 11, 2022). CRUTEM5.0.1.0 (`https://www.metoffice.gov.uk/hadobs/crutem5/data/CRUTEM.5.0.1.0/download.html`; last access, Jun. 11, 2022). HadSST4.0.1.0 200-member ensemble (`https://www.metoffice.gov.uk/hadobs/hadsst4/data/download.html`; last access, May. 20, 2022). HadCRUT5.0.1.0 200-member ensemble (`https://www.metoffice.gov.uk/hadobs/hadcrut5/data/current/download.html`; last access, Jun. 11, 2022). Monthly CMIP6 outputs are from the ESGF portal (`https://esgf-node.llnl.gov/search/cmip6/`; last access, Aug. 16, 2021). $PHA_1$ code and our 200-member ensemble of monthly station LSAT temperature are at `https://doi.org/10.7910/DVN/AA0OM0`.

# APPENDIX A

## Developing synthetic data

We develop synthetic data using both CMIP6 simulations and draws from a multivariate Gaussian process. For CMIP6, we interpolate simulated temperatures using a bi-linear method to locations of weather stations and add a random number of breakpoints with random timing and random magnitude. The number of breakpoints for a given time-series, $n_b$, is specified by drawing a random number from a normal with a mean of 3 and standard deviation of one, truncating values to range between 0 and 6, and then rounding. We next draw $n_b$ independent times across possible time steps with uniform probability and assign a magnitude to each breakpoint that is drawn from $N(-0.05, 1)$. The mean and standard deviation of breakpoint magnitudes are comparable to those reported in Menne et al. (2018), and the non-zero centered distribution introduces biases in long-term trends.

Synthetic temperatures that are correlated in space and time are generated using an AR-1 Multivariate Gaussian Process (MGP),

$$\mathbf{T}_{t+1} = \alpha \mathbf{T}_t + \epsilon. \tag{A1}$$

Vector $\mathbf{T}_t$ represents temperatures at time $t$ in a network of weather stations, for which we choose continental U.S. stations in GHCNmV4. We run Eq. A1 for 700 time steps and discard the first 100 warm-up steps. Varying the system memory, $\alpha$, permits controlling the auto-correlation of generated time series and their differences.

The noise innovation vector, $\epsilon$, follows a Multivariate Gaussian distribution,

$$\epsilon \sim N(\mathbf{0}, \mathbf{\Sigma}), \tag{A2}$$

where $\mathbf{\Sigma}$ is a covariance matrix generated according to $\Sigma_{ij} = (1-\alpha)^2 \exp(-|\Delta d|/\tau)$. The variable $|\Delta d|$ is the arc length, in degrees, between stations $i$ and $j$, and $\tau$ is the decorrelation distance, for which we choose 5°, approximately half of the Rossby deformation radius for the mid-latitude atmosphere. The variance of the noise innovations is a decreasing function of $\alpha$ such that the expected variance of $T$ is constant for $\alpha$ between 0 and 1.

The same seeding of random numbers is used for all synthetic experiments, such that identical breaks are introduced to both CMIP6 models and synthetic data generated from multivariate Gaussian processes.

## APPENDIX B

### Revised pair-wise station homogenization algorithm ($\mathbf{PHA}_1$)

A step-by-step description of $PHA_1$ is provided for purpose of reproducibility. $PHA_1$ generally follows that of Menne and Williams Jr (2009, hereafter $PHA_0$) and Williams et al. (2012, hereafter WMT12). We note where our approach differs from $PHA_0$ and WMT12.

*1. Identify neighbors*

Neighboring stations are first identified. For each target station, we first identify the nearest "NEIGH CLOSE" (80 / **100** / 150 / 200) stations. Numbers in the parenthesis denote possible values of the algorithm parameter inside quotation marks, whereas the one in boldface is our default value (Ensemble member 1 in Table B2). The distance, "NEIGH DIS", is evaluated using one of the following metrics — **difference correlation (1 diff)**, Pearson's correlation (corr), or physical distance on the sphere (near). Where difference correlation is the correlation between month-to-month temperature changes, which minimizes the impact of abrupt breaks in determining the correlation (Peterson et al. 1998).

Before evaluating correlations, temperatures from two stations are masked using the least common coverage, and seasonal cycles are removed, respectively, by subtracting the mean temperature in each month over the entire unmasked period. Note that a small sample size could result in high correlations due to random noise, which is not preferred for station intercomparison. As a result, stations having fewer than "NUM4COV" (60 / **120** / 180) overlapping months with the target station are excluded. When evaluating correlations (1 diff and corr), we also exclude stations whose correlations are smaller than "CORR LIM" (**0.1** / 0.5 / 0.7) with the target station. When using spherical distance (near), we remove seasonal cycles and do not use the "CORR LIM" parameter.

Among eligible neighboring stations, the top "NEIGH FINAL" (20/ **40** / 60 / 80) are first selected. Our algorithm then loops over the remaining stations in descending order. If adding this station increases the number of neighbors for any month that has fewer than "MIN STNS" (5 / **7** / 9) neighbors, the least correlated or the furthest station is replaced. Difference monthly temperature anomalies between the target station and each selected neighbor are calculated.

*2. Perform standard normal homogenization test*

For each difference series, we apply an iterative standard normal homogeneity test (SNHT). The test is performed iteratively between a splitting phase, where the algorithm tests whether each segment of time series contains any further breakpoints, and a merging phase, where the algorithm combines consecutive segments if the combined time series fail to pass SNHT. This process repeats until no more breakpoints can be identified or the number of iterations reaches ten.

Unlike the $PHA_0$ algorithm, which uses the 95% confidence level estimated from white noise series, the revised algorithm uses "SNHT levels" (80%/ **90%** / 95%) estimated from auto-correlated random series.

To estimate updated SNHT thresholds, we first generate n-sample red noise series using an order one auto-regressive process, $X_{t+1} = \alpha X_t + \epsilon$, where $\alpha$ is the memory of the system, for which we loop over 0 to 0.4 at an increment of 0.01, and $n$ is the length of time series that we vary between 5 and 3500. For each combination of $\alpha$ and $N$, 50000 random series are generated and then normalized to zero mean and unit variance.

For each synthetic series, we then calculate lag-1 auto-correlation $\alpha$ and the SNHT statistics, $T_0 = \max\limits_{1\leq v<n}[v\bar{z}_1^2 + (n-v)\bar{z}_2^2]$ (Alexandersson 1986). Here $\bar{z}_1$ and $\bar{z}_2$ are, respectively, the mean over the two periods before and after time step $v$, and the calculation loops $v$ over 1 to n-1 to find the maximum value. For each $n$ value, we calculate the revised SNHT threshold as the 80%, 90%, and 95% quantiles of $T_0$ within 0.1 incremental bins of $\alpha$.

When performing SNHT using revised thresholds, we first evaluate $\alpha$ for each difference series using a sliding window of 100 months, or one third of the time series if shorter than 100 months. We take the median value of the $\alpha$ values sampled across the time series. $\alpha$ is updated in every splitting phase of SNHT, and windows overlapping with any detected breakpoints are discarded in the calculation of median values. This method reduces biases in auto-correlation estimates due to artificial discontinuities. Specific SNHT thresholds not explicitly for a given $n$ and $\alpha$ are estimated using bilinear interpolation (Fig. 3b).

### *3. Identify breakpoints rather than trends*

A check is made as to whether breakpoints identified in step 2 reflect breaks or long-term trends using a Bayesian Information Criterion approach (BIC; Schwarz 1978). Specifically, for a potential breakpoint, $k$, whose timing is $t_k$, we take the two segments on which it centers and calculate the BIC for seven different models. In addition to the five candidate models tested in Menne and

Williams Jr (2009), $PHA_1$ also tests two other models,

$$y_t = \begin{cases} \mu_1 + k_1 t + \epsilon_t & t_{k-1} < t \le t_k \\ \mu_2 + \epsilon_t & t_k < t \le t_{k+1}. \end{cases} \tag{B1}$$

$$y_t = \begin{cases} \mu_1 + \epsilon_t & t_{k-1} < t \le t_k \\ \mu_2 + k_2 t + \epsilon_t & t_k < t \le t_{k+1}. \end{cases} \tag{B2}$$

We fit models using the Theil–Sen estimator (Theil 1950), which uses the median value of slopes between every possible pair of data to obtain a robust fitting that is less affected by outliers. After fitting each model we calculate BIC following,

$$BIC(p) = -n' \log(\frac{SSE}{n'}) + \log(n')p, \tag{B3}$$

where p is the number of parameters in a model, $n'$ is the number of time steps from $t_{k-1}+1$ to $t_{k+1}$, and SSE is the sum of squared error for a particular model fit. A breakpoint is confirmed if any models other than straight lines has the lowest BIC. Otherwise, we exclude it from further analysis. For each confirmed breakpoint, we also record estimates of its normalized magnitude, $\hat{m} = (\mu_2 - \mu_1)/\sqrt{SSE/(n'-1)}$. Unlike as in $PHA_0$, we do not test models containing both a break and long-term trends because such a model results in noisier estimates of the magnitude of breakpoints (see step 7).

*4. Attribute breakpoints to stations*

Breakpoints confirmed in a difference series can be due to breaks in either station involved. As a result, we follow $PHA_0$ to attribute breaks to individual stations using a count-down method that prioritizes stations having identifiable breakpoints in step 3 against more neighboring stations. This procedure is performed across all time steps. Specifically, at time step $t$, we count the number of neighbors, $\tilde{n}$, with which a particular station shows a break. When two breaks involve stations that are mutually targets and neighbors, we exclude one of them to avoid double counting.

After forming a list of breakpoint counts, we find the station and the timing having the highest count and associate it with the breakpoint. The counts of neighboring stations that were originally associated with this breakpoint at this timing are decreased by one. Furthermore, the count of the station originally having the highest count is decreased by $\tilde{n}$ in order to facilitate finding the next highest count. The procedure is repeated until no count is greater than one, reflecting the fact that we require two neighboring stations at a time step to confirm a target as the source of a break.

*5. Combine near-in-time breakpoints*

Although breakpoints are assigned to individual stations, the identified timing maybe uncertain. We, therefore, combine near-in-time breakpoints to account for timing errors. (Menne and Williams Jr 2009) estimated the timing error by realizing 100-sample random time series with breakpoints of different magnitudes added at the 50th time step. They performed SNHT to each of the synthetic series and calculated the error of the timing of identified breakpoints, which decreases with the magnitude of breaks. Although timing error would depends on autocorrelation, we keep its estimation to be the same as Menne and Williams Jr (2009) for simplicity.

For each station, each attributed breakpoint is assigned with an epoch, whose length is the 90% / **92%** / 95% interval of timing error, "AMPLOC PCT". Breakpoints whose confidence intervals overlap within a particular station record are combined together. Starting from the breakpoint that has the largest absolute magnitude, we combine all breakpoints whose epoch overlap with that of the selected breakpoint. The process the continues with selecting the largest magnitude among uncombined breakpoints until no further combinations are possible.

*6. Estimate adjustment magnitudes*

Steps 1–5 identify a collection of undocumented breakpoints in a network of temperature series, which is then used to estimate required adjustments. The same as $\mathrm{PHA}_0$, we adjust the combined effect when breakpoints cluster within "ADJ MINLIN" (12 / **24** / 36) months.

We estimate the required adjustments for each breakpoint independently. Taking breakpoint $k$ for station $S$ as an example, we first subset the time interval $t_{k-1}+1$ to $t_{k+1}$. If a neighbor of station S does not contain any breaks during this interval, we then use the corresponding difference series from $t_{k-1}+1$ to $t_{k+1}$ to estimate the magnitude using the change point model in step 3 that has the lowest BIC for this breakpoint. If a neighbor contains breakpoints, but none are within "ADJ WINDOW" (**6** / 12 / 24 / 36) months before and after the target break, we estimate an adjustment using the difference series from the neighbor's last break before the target and the first break after. Otherwise, no adjustments are estimated. Looping over all neighbors results in a collection of estimated adjustments. The method then can choose whether or not to trim, "ADJ OUTLIER" (0 / **1**), these estimates using a Tukey method (Tukey 1977). The Tukey method first finds the median ($Q_2$) and the first ($Q_1$) and third quartiles ($Q_3$). It then trims off all samples that are smaller than $Q_1 - k(Q_2 - Q_1)$ or larger than $Q_3 + k(Q_3 - Q_2)$, where k = 1.64, a value used by Williams et al. (2012). If more than "ADJ MINPAIR" (**2** / 3 / 4 / 5) samples remain, another Tukey method is applied to these remaining samples. If $Q_1 - k(Q_2 - Q_1)$ and $Q_3 + k(Q_3 - Q_2)$ are of the same sign, we use "ADJ EST" (median / mean / average of the 25% and 75% quartiles) as the final adjustment. Otherwise, this breakpoint is discarded. The estimation of adjustments runs two times, with the first time discarding unadjustable breaks, and the second time estimating adjustments using only adjustable breaks. Following $PHA_0$, $PHA_1$ also adjusts temperature series relative to values in the ending period.

*7. Iterate*

Step 1-6 removes heterogeneity in a network of station temperatures. Whereas the original algorithm only runs one iteration, the revised algorithm allows for running multiple iterations, and the new iteration simply starts from adjusted temperatures in the last iteration. Empirically, running two iterations would be sufficient, because the third iteration only leads to minor changes (see section 4).

Table B1. Parameters in the revised algorithm. Except for the first three rows, other parameters are identical to those in Williams et al. (2012).

| Parameter | Meaning |
|---|---|
| ADJ EST | Methods to determine adjustments from multiple pairwise estimates |
| ADJ MINLEN | Minimum length of data period that can be adjusted |
| ADJ MINPAIR | Minimum number of non-problematic neighbors to estimate adjustments |
| ADJ OUTLIER | Whether trim breakpoint magnitude estimate before calculate mean values |
| ADJ WINDOW | Minimum number of months on two sides of breakpoints to estimate adjustments |
| AMPLOC PCT | Confidence window used to conflate breakpoints |
| BIC PENALTY | Regulation approach when fitting seven change-point models |
| CONFIRM | Number of neighbors required to confirm a breakpoint |
| CORR LIM | Minimum correlation to be identified as a neighbor |
| MIN STNS | Minimum number neighbors with coincident data |
| NEIGH CLOSE | Maximum number of neighboring series to consider |
| NEIGH CORR | Similarity matrix used for ranking neighbors |
| NEIGH FINAL | Final (maximum) number of neighbors per station |
| SNHT THRES | Confidence level of the standard normal homogeneous test (SNHT) |

Table B2. Parameters in individual ensemble members. Member 1 is the parameter combination for the original algorithm, whose values are from Williams et al. (2012). Member 2–99 form randomly perturbing PHA parameters.

| En. No. | 1 | 2 | 3 | 4 | 5 | 6 | 7 | 8 | 9 | 10 | 11 | 12 | 13 |
|---|---|---|---|---|---|---|---|---|---|---|---|---|---|
| ADJ EST | Med | Avg | Qavg | Avg | Med | Qavg | Med | Qavg | Med | Med | Qavg | Med | Qavg |
| ADJ MINLEN | 18 | 18 | 18 | 24 | 18 | 18 | 18 | 18 | 18 | 18 | 18 | 24 | 24 |
| ADJ MINPAIR | 2 | 4 | 4 | 4 | 2 | 5 | 5 | 4 | 5 | 2 | 5 | 3 | 3 |
| ADJ OUTLIER | 1 | 1 | 1 | 0 | 0 | 1 | 0 | 1 | 1 | 1 | 1 | 0 | 0 |
| ADJ WINDOW | 0 | 0 | 0 | 0 | 0 | 0 | 0 | 0 | 0 | 0 | 0 | 0 | 0 |
| AMPLOC PCT | 92 | 95 | 92 | 90 | 95 | 95 | 95 | 92 | 95 | 92 | 90 | 90 | 92 |
| BIC PENALTY | BIC | none | BIC | BIC | BIC | none | AIC | none | AIC | BIC | none | none | none |
| CONFIRM | 2 | 2 | 2 | 2 | 2 | 3 | 3 | 3 | 2 | 2 | 4 | 3 | 3 |
| CORR LIM | 0.1 | 0.5 | 0.1 | 0.1 | 0.1 | 0.1 | 0.7 | 0.1 | 0.1 | 0.1 | 0.5 | 0.1 | 0.5 |
| MIN STNS | 7 | 7 | 7 | 9 | 9 | 5 | 7 | 5 | 9 | 9 | 5 | 9 | 7 |
| NEIGH CLOSE | 100 | 80 | 80 | 80 | 100 | 100 | 100 | 200 | 150 | 100 | 200 | 150 | 80 |
| NEIGH CORR | 1diff | 1diff | near | 1diff | 1diff | near | near | 1diff | near | near | near | 1diff | near |
| NEIGH FINAL | 40 | 20 | 20 | 20 | 20 | 40 | 20 | 20 | 40 | 40 | 40 | 40 | 20 |
| SNHT THRES | 95 | 97.5 | 97.5 | 97.5 | 95 | 90 | 90 | 90 | 97.5 | 95 | 90 | 95 | 95 |
| En. No. | 14 | 15 | 16 | 17 | 18 | 19 | 20 | 21 | 22 | 23 | 24 | 25 | 26 |
| ADJ EST | Qavg | Qavg | Avg | Avg | Med | Avg | Med | Qavg | Qavg | Med | Qavg | Avg | Avg |
| ADJ MINLEN | 24 | 24 | 18 | 24 | 24 | 18 | 18 | 18 | 24 | 24 | 18 | 18 | 18 |
| ADJ MINPAIR | 4 | 4 | 2 | 5 | 2 | 2 | 5 | 3 | 2 | 3 | 5 | 4 | 2 |
| ADJ OUTLIER | 0 | 0 | 0 | 0 | 1 | 0 | 0 | 0 | 1 | 0 | 1 | 1 | 0 |
| ADJ WINDOW | 0 | 0 | 0 | 0 | 0 | 0 | 0 | 0 | 0 | 0 | 0 | 0 | 120 |
| AMPLOC PCT | 90 | 95 | 95 | 92 | 95 | 92 | 95 | 90 | 90 | 95 | 90 | 92 | 92 |
| BIC PENALTY | none | AIC | BIC | AIC | BIC | none | none | BIC | none | BIC | AIC | AIC | none |
| CONFIRM | 3 | 3 | 3 | 4 | 4 | 2 | 4 | 2 | 4 | 3 | 5 | 5 | 2 |
| CORR LIM | 0.7 | 0.5 | 0.1 | 0.5 | 0.1 | 0.7 | 0.7 | 0.5 | 0.5 | 0.1 | 0.1 | 0.1 | 0.7 |
| MIN STNS | 5 | 7 | 5 | 7 | 9 | 9 | 5 | 9 | 7 | 7 | 9 | 9 | 7 |
| NEIGH CLOSE | 150 | 100 | 150 | 80 | 80 | 200 | 200 | 200 | 150 | 100 | 150 | 80 | 200 |
| NEIGH CORR | near | near | 1diff | 1diff | near | 1diff | near | corr | 1diff | near | 1diff | near | 1diff |
| NEIGH FINAL | 40 | 40 | 20 | 40 | 60 | 40 | 40 | 20 | 60 | 20 | 80 | 60 | 20 |
| SNHT THRES | 95 | 90 | 95 | 95 | 95 | 95 | 97.5 | 90 | 95 | 97.5 | 90 | 95 | 97.5 |
| En. No. | 27 | 28 | 29 | 30 | 31 | 32 | 33 | 34 | 35 | 36 | 37 | 38 | 39 |
| ADJ EST | Med | Qavg | Qavg | Avg | Qavg | Med | Med | Qavg | Qavg | Avg | Qavg | Med | Qavg |
| ADJ MINLEN | 24 | 18 | 24 | 18 | 18 | 18 | 18 | 36 | 18 | 18 | 36 | 36 | 24 |
| ADJ MINPAIR | 5 | 5 | 3 | 4 | 5 | 4 | 4 | 2 | 2 | 5 | 4 | 4 | 2 |
| ADJ OUTLIER | 0 | 1 | 1 | 1 | 1 | 0 | 1 | 0 | 0 | 0 | 1 | 0 | 1 |
| ADJ WINDOW | 0 | 0 | 0 | 0 | 120 | 0 | 0 | 0 | 0 | 0 | 0 | 0 | 0 |
| AMPLOC PCT | 92 | 92 | 92 | 92 | 95 | 95 | 92 | 90 | 92 | 95 | 92 | 95 | 90 |
| BIC PENALTY | none | AIC | AIC | AIC | AIC | BIC | BIC | AIC | BIC | BIC | AIC | BIC | none |
| CONFIRM | 3 | 5 | 5 | 3 | 2 | 3 | 4 | 2 | 5 | 3 | 2 | 2 | 3 |
| CORR LIM | 0.5 | 0.7 | 0.1 | 0.5 | 0.7 | 0.1 | 0.5 | 0.5 | 0.1 | 0.5 | 0.1 | 0.5 | 0.5 |
| MIN STNS | 5 | 5 | 9 | 7 | 5 | 7 | 9 | 9 | 7 | 7 | 7 | 9 | 9 |
| NEIGH CLOSE | 200 | 100 | 80 | 200 | 150 | 100 | 100 | 200 | 150 | 150 | 100 | 200 | 200 |
| NEIGH CORR | corr | near | corr | corr | 1diff | 1diff | near | near | 1diff | corr | 1diff | 1diff | near |
| NEIGH FINAL | 40 | 80 | 80 | 60 | 20 | 60 | 80 | 20 | 80 | 40 | 20 | 20 | 80 |
| SNHT THRES | 97.5 | 97.5 | 97.5 | 97.5 | 95 | 90 | 90 | 95 | 90 | 97.5 | 90 | 97.5 | 95 |
| En. No. | 40 | 41 | 42 | 43 | 44 | 45 | 46 | 47 | 48 | 49 | 50 | 51 | 52 |
| ADJ EST | Qavg | Med | Med | Qavg | Qavg | Qavg | Qavg | Avg | Med | Med | Avg | Med | Avg |
| ADJ MINLEN | 24 | 24 | 24 | 36 | 36 | 24 | 24 | 18 | 18 | 24 | 18 | 18 | 24 |
| ADJ MINPAIR | 4 | 4 | 3 | 3 | 4 | 2 | 5 | 3 | 5 | 5 | 5 | 4 | 5 |
| ADJ OUTLIER | 0 | 0 | 0 | 0 | 0 | 1 | 0 | 1 | 0 | 1 | 1 | 0 | 0 |
| ADJ WINDOW | 0 | 0 | 0 | 0 | 0 | 120 | 0 | 0 | 120 | 0 | 120 | 120 | 0 |
| AMPLOC PCT | 95 | 92 | 95 | 92 | 90 | 92 | 90 | 92 | 95 | 92 | 95 | 90 | 95 |
| BIC PENALTY | none | AIC | BIC | AIC | AIC | none | AIC | AIC | BIC | BIC | BIC | none | none |
| CONFIRM | 5 | 4 | 3 | 3 | 2 | 2 | 4 | 5 | 3 | 5 | 4 | 2 | 2 |
| CORR LIM | 0.5 | 0.5 | 0.5 | 0.5 | 0.5 | 0.1 | 0.1 | 0.5 | 0.5 | 0.5 | 0.5 | 0.1 | 0.5 |
| MIN STNS | 5 | 9 | 5 | 7 | 7 | 5 | 5 | 7 | 7 | 7 | 9 | 5 | 7 |
| NEIGH CLOSE | 200 | 150 | 150 | 100 | 80 | 100 | 80 | 100 | 80 | 200 | 200 | 80 | 200 |
| NEIGH CORR | 1diff | 1diff | near | 1diff | corr | near | 1diff | corr | 1diff | corr | 1diff | near | corr |
| NEIGH FINAL | 40 | 80 | 80 | 40 | 20 | 40 | 80 | 60 | 20 | 60 | 40 | 40 | 60 |
| SNHT THRES | 95 | 90 | 95 | 95 | 90 | 97.5 | 90 | 97.5 | 90 | 95 | 90 | 97.5 | 97.5 |

Table B2. Continue.

| En. No. | 53 | 54 | 55 | 56 | 57 | 58 | 59 | 60 | 61 | 62 | 63 | 64 | 65 |
|---|---|---|---|---|---|---|---|---|---|---|---|---|---|
| ADJ EST | Med | Qavg | Med | Qavg | Avg | Med | Med | Qavg | Qavg | Qavg | Avg | Qavg | Qavg |
| ADJ MINLEN | 36 | 36 | 36 | 24 | 36 | 18 | 18 | 36 | 36 | 36 | 24 | 36 | 36 |
| ADJ MINPAIR | 3 | 3 | 4 | 4 | 4 | 2 | 2 | 2 | 4 | 3 | 5 | 5 | 4 |
| ADJ OUTLIER | 1 | 1 | 0 | 1 | 0 | 1 | 1 | 1 | 1 | 1 | 1 | 0 | 0 |
| ADJ WINDOW | 120 | 0 | 0 | 0 | 0 | 0 | 120 | 0 | 0 | 0 | 120 | 0 | 0 |
| AMPLOC PCT | 95 | 92 | 95 | 95 | 95 | 92 | 92 | 92 | 92 | 92 | 95 | 90 | 95 |
| BIC PENALTY | AIC | AIC | BIC | AIC | none | BIC | AIC | AIC | BIC | none | BIC | none | AIC |
| CONFIRM | 2 | 2 | 3 | 2 | 4 | 5 | 2 | 3 | 2 | 3 | 4 | 4 | 3 |
| CORR LIM | 0.1 | 0.7 | 0.7 | 0.5 | 0.7 | 0.5 | 0.1 | 0.1 | 0.1 | 0.1 | 0.1 | 0.1 | 0.7 |
| MIN STNS | 9 | 5 | 7 | 7 | 7 | 7 | 9 | 9 | 5 | 5 | 5 | 9 | 7 |
| NEIGH CLOSE | 100 | 200 | 100 | 80 | 100 | 80 | 150 | 150 | 150 | 100 | 80 | 200 | 80 |
| NEIGH CORR | near | 1diff | 1diff | 1diff | near | corr | 1diff | near | corr | 1diff | 1diff | 1diff | 1diff |
| NEIGH FINAL | 20 | 80 | 40 | 80 | 60 | 60 | 40 | 60 | 40 | 60 | 60 | 60 | 20 |
| SNHT THRES | 97.5 | 97.5 | 97.5 | 90 | 90 | 90 | 90 | 90 | 97.5 | 90 | 90 | 95 | 97.5 |
| En. No. | 66 | 67 | 68 | 69 | 70 | 71 | 72 | 73 | 74 | 75 | 76 | 77 | 78 |
| ADJ EST | Qavg | Med | Med | Med | Avg | Med | Med | Med | Qavg | Qavg | Qavg | Qavg | Avg |
| ADJ MINLEN | 24 | 36 | 36 | 36 | 18 | 18 | 36 | 24 | 36 | 36 | 36 | 18 | 36 |
| ADJ MINPAIR | 3 | 3 | 5 | 5 | 2 | 2 | 5 | 4 | 2 | 2 | 3 | 5 | 3 |
| ADJ OUTLIER | 1 | 1 | 1 | 1 | 0 | 1 | 1 | 1 | 0 | 1 | 1 | 0 | 1 |
| ADJ WINDOW | 120 | 120 | 0 | 0 | 120 | 120 | 0 | 0 | 120 | 0 | 0 | 120 | 0 |
| AMPLOC PCT | 92 | 92 | 95 | 95 | 90 | 90 | 95 | 92 | 95 | 95 | 95 | 90 | 90 |
| BIC PENALTY | BIC | none | none | BIC | BIC | AIC | AIC | none | none | BIC | AIC | AIC | none |
| CONFIRM | 4 | 2 | 5 | 3 | 4 | 2 | 2 | 2 | 2 | 4 | 3 | 3 | 4 |
| CORR LIM | 0.7 | 0.7 | 0.1 | 0.1 | 0.5 | 0.5 | 0.5 | 0.5 | 0.7 | 0.1 | 0.1 | 0.1 | 0.5 |
| MIN STNS | 7 | 9 | 7 | 5 | 7 | 9 | 9 | 9 | 9 | 5 | 7 | 9 | 5 |
| NEIGH CLOSE | 80 | 80 | 150 | 80 | 80 | 80 | 150 | 80 | 200 | 150 | 200 | 80 | 150 |
| NEIGH CORR | near | 1diff | near | near | near | corr | 1diff | near | 1diff | corr | near | corr | corr |
| NEIGH FINAL | 40 | 20 | 80 | 80 | 60 | 60 | 60 | 80 | 40 | 40 | 80 | 20 | 40 |
| SNHT THRES | 97.5 | 90 | 90 | 95 | 90 | 97.5 | 95 | 90 | 97.5 | 90 | 90 | 95 | 95 |
| En. No. | 79 | 80 | 81 | 82 | 83 | 84 | 85 | 86 | 87 | 88 | 89 | 90 | 91 |
| ADJ EST | Qavg | Qavg | Qavg | Qavg | Qavg | Qavg | Qavg | Med | Avg | Avg | Med | Qavg | Avg |
| ADJ MINLEN | 18 | 24 | 36 | 18 | 24 | 18 | 18 | 18 | 18 | 24 | 24 | 18 | 24 |
| ADJ MINPAIR | 5 | 2 | 3 | 2 | 3 | 5 | 3 | 3 | 3 | 2 | 3 | 2 | 2 |
| ADJ OUTLIER | 0 | 1 | 0 | 0 | 1 | 0 | 0 | 1 | 1 | 1 | 0 | 1 | 0 |
| ADJ WINDOW | 120 | 120 | 0 | 60 | 120 | 120 | 0 | 120 | 120 | 120 | 0 | 60 | 120 |
| AMPLOC PCT | 95 | 92 | 92 | 90 | 90 | 92 | 95 | 95 | 95 | 95 | 90 | 95 | 95 |
| BIC PENALTY | none | BIC | BIC | BIC | none | BIC | none | AIC | BIC | none | AIC | none | AIC |
| CONFIRM | 5 | 4 | 3 | 2 | 5 | 3 | 4 | 5 | 5 | 5 | 4 | 2 | 5 |
| CORR LIM | 0.5 | 0.5 | 0.7 | 0.5 | 0.1 | 0.1 | 0.7 | 0.5 | 0.5 | 0.1 | 0.5 | 0.5 | 0.1 |
| MIN STNS | 9 | 5 | 7 | 5 | 5 | 9 | 7 | 5 | 5 | 5 | 5 | 7 | 9 |
| NEIGH CLOSE | 150 | 100 | 200 | 100 | 80 | 80 | 150 | 80 | 80 | 100 | 150 | 100 | 80 |
| NEIGH CORR | 1diff | 1diff | near | near | 1diff | corr | 1diff | near | 1diff | corr | near | 1diff | 1diff |
| NEIGH FINAL | 60 | 80 | 80 | 20 | 60 | 60 | 20 | 40 | 60 | 80 | 20 | 20 | 80 |
| SNHT THRES | 95 | 97.5 | 90 | 90 | 97.5 | 95 | 95 | 97.5 | 97.5 | 95 | 97.5 | 90 | 97.5 |
| En. No. | 92 | 93 | 94 | 95 | 96 | 97 | 98 | 99 | 100 | | | | |
| ADJ EST | Qavg | Med | Avg | Med | Qavg | Qavg | Med | Med | Med | | | | |
| ADJ MINLEN | 24 | 18 | 24 | 18 | 36 | 18 | 36 | 18 | 36 | | | | |
| ADJ MINPAIR | 5 | 2 | 4 | 3 | 4 | 5 | 4 | 2 | 2 | | | | |
| ADJ OUTLIER | 0 | 0 | 1 | 0 | 1 | 1 | 0 | 1 | 0 | | | | |
| ADJ WINDOW | 0 | 120 | 60 | 60 | 120 | 120 | 0 | 120 | 120 | | | | |
| AMPLOC PCT | 95 | 92 | 95 | 90 | 90 | 95 | 95 | 90 | 92 | | | | |
| BIC PENALTY | none | none | BIC | BIC | BIC | BIC | BIC | BIC | none | | | | |
| CONFIRM | 4 | 5 | 2 | 2 | 2 | 2 | 4 | 2 | 4 | | | | |
| CORR LIM | 0.5 | 0.1 | 0.7 | 0.7 | 0.7 | 0.5 | 0.7 | 0.5 | 0.1 | | | | |
| MIN STNS | 5 | 5 | 9 | 9 | 5 | 5 | 9 | 9 | 5 | | | | |
| NEIGH CLOSE | 150 | 200 | 200 | 100 | 150 | 100 | 80 | 150 | 80 | | | | |
| NEIGH CORR | near | 1diff | 1diff | 1diff | 1diff | 1diff | 1diff | 1diff | 1diff | | | | |
| NEIGH FINAL | 20 | 80 | 20 | 20 | 80 | 80 | 40 | 80 | 40 | | | | |
| SNHT THRES | 95 | 95 | 95 | 97.5 | 97.5 | 95 | 90 | 90 | 90 | | | | |

## References

Alexandersson, H., 1986: A homogeneity test applied to precipitation data. *Journal of climatology*, **6 (6)**, 661–675.

Chan, D., G. Gebbie, and P. Huybers, 2023: Global and regional discrepancies between early-twentieth-century coastal air and sea surface temperature detected by a coupled energy-balance analysis. *Journal of Climate*, **36 (7)**, 2205–2220.

Costa, A. C., and A. Soares, 2009: Homogenization of climate data: review and new perspectives using geostatistics. *Mathematical geosciences*, **41 (3)**, 291–305.

Cowtan, K., R. Rohde, and Z. Hausfather, 2018: Evaluating biases in sea surface temperature records using coastal weather stations. *Quarterly Journal of the Royal Meteorological Society*, **144 (712)**, 670–681.

Eyring, V., S. Bony, G. A. Meehl, C. A. Senior, B. Stevens, R. J. Stouffer, and K. E. Taylor, 2016: Overview of the Coupled Model Intercomparison Project Phase 6 (CMIP6) experimental design and organization. *Geoscientific Model Development*, **9 (5)**, 1937–1958.

Kadow, C., D. M. Hall, and U. Ulbrich, 2020: Artificial intelligence reconstructs missing climate information. *Nature Geoscience*, 1–6.

Kennedy, J., N. Rayner, C. Atkinson, and R. Killick, 2019: An ensemble data set of sea surface temperature change from 1850: The Met Office Hadley Centre HadSST. 4.0.0.0 data set. *Journal of Geophysical Research: Atmospheres*, **124 (14)**, 7719–7763.

Lawrimore, J. H., M. J. Menne, B. E. Gleason, C. N. Williams, D. B. Wuertz, R. S. Vose, and J. Rennie, 2011: An overview of the global historical climatology network monthly mean temperature data set, version 3. *Journal of Geophysical Research: Atmospheres*, **116 (D19)**.

Meinshausen, N., S. Sippel, E. M. Fischer, V. Humphrey, R. A. Rohde, I. E. de Vries, and R. Knutti, 2022: New land-vs. ocean based global mean temperature reconstructions reveal high consistency except for early 20 th century ocean cold anomaly. *Fall Meeting 2022*, AGU.

Menne, M. J., C. N. Williams, B. E. Gleason, J. J. Rennie, and J. H. Lawrimore, 2018: The global historical climatology network monthly temperature dataset, version 4. *Journal of Climate*, **31 (24)**, 9835–9854.

Menne, M. J., and C. N. Williams Jr, 2009: Homogenization of temperature series via pairwise comparisons. *Journal of Climate*, **22 (7)**, 1700–1717.

Morice, C. P., and Coauthors, 2021: An updated assessment of near-surface temperature change from 1850: the hadcrut5 data set. *Journal of Geophysical Research: Atmospheres*, **126 (3)**, e2019JD032 361.

Osborn, T. J., P. D. Jones, D. H. Lister, C. P. Morice, I. R. Simpson, J. Winn, E. Hogan, and I. C. Harris, 2021: Land surface air temperature variations across the globe updated to 2019: The CRUTEM5 data set. *Journal of Geophysical Research: Atmospheres*, **126 (2)**, e2019JD032 352.

Peterson, T. C., and Coauthors, 1998: Homogeneity adjustments of in situ atmospheric climate data: a review. *International Journal of Climatology: A Journal of the Royal Meteorological Society*, **18 (13)**, 1493–1517.

Rohde, R., and Coauthors, 2013a: Berkeley earth temperature averaging process, geoinfor. geostat.-an overview, 1, 2. *Geoinformatics Geostatistics An Overview*, **1 (2)**, 20–100.

Rohde, R., and Coauthors, 2013b: A new estimate of the average earth surface land temperature spanning 1753 to 2011. geoinfor geostat: An overview 1: 1.

Schwarz, G., 1978: Estimating the dimension of a model. *The annals of statistics*, 461–464.

Theil, H., 1950: A rank-invariant method of linear and polynomial regression analysis. *Indagationes mathematicae*, **12 (85)**, 173.

Trewin, B., 2010: Exposure, instrumentation, and observing practice effects on land temperature measurements. *Wiley Interdisciplinary Reviews: Climate Change*, **1 (4)**, 490–506.

Tukey, J., 1977: Exploratory data analysis. addison-wesley, reading, 688 pp.

Venema, V. K., and Coauthors, 2012: Benchmarking homogenization algorithms for monthly data. *Climate of the Past*, **8 (1)**, 89–115.

Williams, C. N., M. J. Menne, and P. W. Thorne, 2012: Benchmarking the performance of pairwise homogenization of surface temperatures in the united states. *Journal of Geophysical Research: Atmospheres*, **117 (D5)**.